Structures and Reactions of P_2N_2: A Hybrid of Elemental N_2 and P_4?

Ohyun Kwon, Philip M. Almond, and Michael L. McKee*

Department of Chemistry, Auburn University, Auburn, Alabama 36849

Received: March 14, 2002; In Final Form: April 23, 2002

A systematic study of all possible tetraatomic P_2N_2 structures has been made at the B3LYP/6-311+G(2df) and CASPT2(12e,12o)/ANO-L levels. A closed-shell butterfly C_{2v} structure (**A**) is predicted to have the lowest energy on the tetraatomic P_2N_2 potential energy surface. The energies for dissociation of P_2N_2 to two $P{\equiv}N$ or to N_2 and P_2 have been examined. A closed-shell quasi-tetrahedral C_{2v} structure of P_2N_2 (**B**) and a linear open-shell singlet $P-N{\equiv}N-P$ (**E***) have been found to be kinetically stable to fragmentation or rearrangement at the CASPT2/ANO-L level. Several transition states have significant biradical character which reflects the orbital crossings that are found along reaction paths of least motion. The fragmentation reaction of $P-N{\equiv}N-P$ to $2P{\equiv}N$ involves a trans-bent transition state that has a strong similarity to a known transition metal reaction.

Introduction

The chemistry of nitrogen and phosphorus has attracted considerable attention from scientists due to their central role in biology and the environment.[1] Although both nitrogen and phosphorus atoms belong to group 15 of the periodic table, their chemistries are quite different. The most abundant form of nitrogen occurs as N_2 due to the extraordinary stability of a triple bond, whereas tetrahedral P_4 (elemental white phosphorus) dissociates to two P_2 molecules only at high temperature.

In the last 2 decades, isomers of N_4 such as tetraazatetrahedrane as well as larger nitrogen clusters (N_n, $n > 4$), have been considered as possible candidate high energy-density materials.[2−19] Previous theoretical studies have characterized the lowest-energy conformer of N_4 as the triplet open-chain C_{2h} structure.[6,8] On the other hand, the tetrahedral N_4 is a local minimum which is the most stable singlet on the N_4 potential energy surface (PES).[8−10,13,15] In particular, tetrahedral N_4 has been the primary subject of previous theoretical studies[2−10,12,14,15,17,18] because the dissociation of N_4 into two N_2 molecules is a Woodward–Hoffmann symmetry-forbidden reaction.[20] Dunn and Morokuma characterized a transition state for the exothermic dissociation of tetrahedral N_4 into two N_2 and estimated the activation energy barrier to be 63 kcal/mol at the CASSCF(12e,12o) level,[7] which indicates that N_4 is a metastable species and should be kinetically stable. Recent experimental studies confirmed the existence of N_4 in the nitrogen plasma as well as in liquid and solid nitrogen.[16,18]

Most recently, the experimental detection of tetranitrogen was reported using neutralization–reionization mass spectrometry.[21] The tetrahedral N_4 isomer could be eliminated as the species observed on the basis of isotopic substitution reactions. The authors considered the open-chained triplet N_4 species as the most likely candidate for the observed species.

There have also been numerous theoretical calculations on the isomers of P_4, which have shown that tetrahedral P_4 is undoubtedly the lowest energy isomer followed by the butterfly D_{2d} structure.[22]

P_2N_2, isovalent to P_4 and N_4, could be another possible candidate high energy-density material because P_2N_2 is expected to be a bridge between P_4 and N_4 with intermediate physical properties. Even though P_2N_2 has not been detected experimentally, it is possible that $P{\equiv}N$, a well-known interstellar species,[23] could dimerize to form P_2N_2 in the dense interstellar medium. A matrix-isolation experiment established the existence of $(PN)_3$, a trimer of $P{\equiv}N$ unit.[24] Schnöckel and co-workers[25] reported IR experiments on $P{\equiv}N$ and P_3N_3 as well as SCF calculations of $(PN)_x$ ($x = 1, 2, 3$). They concluded that the most stable structure of P_2N_2 was a van der Waals complex of two $P{\equiv}N$ molecules with D_{2h} symmetry.[25]

In the present study, quantum mechanical calculations were used to determined the low-energy structures of P_2N_2 isomers as well as rearrangement pathways among isomers and fragmentation to $P{\equiv}N$, N_2, and P_2.

Computational Details

Two different theoretical approaches were used in this study. First, density functional theory (DFT)[26] at the B3LYP/6-311+G(2df) level[27] was applied to obtain optimized geometries of all stationary points. All geometries were analyzed by computing vibrational frequencies and characterized as minima with no imaginary frequencies or as transition states with one imaginary frequency. The transition vector of each transition state was animated by the MOLDEN program.[28] If the pathway connecting the transition state to reactant and product was not obvious, a small distortion along the transition vector was added to the transition state geometry, which was then reoptimized to the corresponding reactant or product. Zero-point and heat capacity corrections were also obtained from vibrational frequency calculations. All DFT calculations were carried out with the Gaussian 98 program.[29]

Many of the stationary points in this study can be characterized as biradicals, which indicates that there are significant contributions from more than one electronic configuration. DFT methods are known to be capable of describing singlet biradicals.[30] A general approach is to optimize geometries with an unrestricted DFT method (UDFT) where the α and β spins are allowed to be mixed. UDFT solutions for singlet biradical structures can be found with the aid of "guess = mix" option in Gaussian 98 where the spin-squared value ($\langle S^2 \rangle$) may approach 1.0 for a strong singlet biradical rather than the correct

Structures and Reactions of P$_2$N$_2$

J. Phys. Chem. A, Vol. 106, No. 29, 2002 **6865**

TABLE 1: Relative Energies (kcal/mol) of Species on the P$_2$N$_2$ Potential Energy Surface

| | | | | | CASPT2^c | | | | |
| | | | | | | | | orbital occupation^d | |
	PG	DFT^a	⟨S^2⟩^{b}	DFT +ZPC^a	CASPT2	+ZPC^e	ΔG(298K)^f	HOMO	LUMO
A	C_{2v}	0.0	0	0.0	0.0	0.0	0.0	1.912	0.086
B	C_{2v}	9.0	0	9.0	2.0	2.0	2.1	1.920	0.071
C	C_{2v}	35.2	0	35.2	24.0	24.3	23.6	1.816	0.166
C*	C_{2v}	35.2	0.06	34.9	23.9	23.5	23.1	1.816	0.169
D	D_{2h}	40.6	0	40.2	32.1	31.7	30.8	1.878	0.115
E	$D_{\infty h}$	25.1	0	25.8	17.5	18.2	19.0	1.005	1.005
E*	$D_{\infty h}$	11.9	1.04	12.6	17.4	18.1	18.9	1.006	1.006
E(t)^g	$D_{\infty h}$	7.6	2.08	8.3	4.2	4.9	5.1	0.995	0.995
TS1	C_{2h}	3.1	0	2.6	3.9	3.5	3.5	1.911	0.073
TS2*	C_{2v}	38.4	0.85	37.0	36.1	34.8	34.4	1.782	0.202
TS3*	C_{2v}	48.2	0.98	47.3	42.0	41.0	40.7	1.212	0.778
TS4	C_1	71.2	0	69.4	63.5	61.7	61.0	1.847	0.158
TS5	C_1	75.7	0	74.6	75.9	74.8	74.2	1.871	0.119
TS5*	C_1	64.3	1.02	62.6	66.5	64.8	63.9	1.022	0.964
TS6*	C_1	49.4	1.00	48.0	45.7	44.3	43.8	1.142	0.849
TS7	C_{2v}	49.7	0	49.8	40.8	40.8	40.7	1.667	0.320
TS7*	C_2	45.2	0.89	44.4	37.2	36.4	35.8	1.591	0.394
TS8	C_{2h}	41.9	0	40.4	32.3	30.9	30.0	1.742	0.253
TS8*	C_{2h}	40.8	0.38	39.0	31.5	29.7	29.5	1.774	0.219
TS9	C_s	62.4	0	61.5	54.2	53.3	52.5	1.832	0.187
TS10*	C_s	37.3	0.34	36.0	23.1	21.7	21.1	1.819	0.163
TS11	C_2	24.1	0	22.9	20.3	19.2	18.1	1.900	0.084
N$_2$+P$_2$		−51.5		−52.6	−63.7	−64.8	−73.2		
2P≡N		2.3		0.6	−8.1	−9.8	−19.2		
PNN+P(^{4}S)		61.2		60.4	43.1	42.3	34.1		
AlNNAl **X**	$D_{\infty h}$	0.0	0	0.0					
AlNNAl **X***	$D_{\infty h}$	−11.7	1.00	−11.6					
AlNNAl **X(t)^g**	$D_{\infty h}$	−15.9	2.01	−15.8					
SiNNSi **Y**	$D_{\infty h}$	0.0	0	0.0					
SiNNSi **Y(t)^g**	$D_{\infty h}$	51.3	2.03	50.4					
SNNS **Z**	$D_{\infty h}$	0.0	0	0.0					
SNNS **Z(t)^g**	$D_{\infty h}$	65.6	2.02	64.4					

^{a} At the B3LYP/6-311+G(2df) level. ^{b} Spin-squared value at the B3LYP/6-311+G(2df) level before spin projection. ^{c} CASPT2(12e,12o)/ANO-L//B3LYP/6-311+G(2df). ^{d} Natural orbital populations for the two orbitals which deviate most from 2.0 (HOMO) and 0.0 (LUMO). ^{e} Zero-point corrections are computed at the B3LYP/6-311+G(2df) level. ^{f} Heat capacity corrections and entropies computed at the B3LYP/6-311+G(2df) level at 298K are used with relative energies at the CASPT2(12e,12o)/ANO-L//B3LYP/6-311+G(2df)+ZPC level to compute free energies. ^{g} Triplet state.

value of 0.0. Nevertheless, many studies have shown results which closely match those of more sophisticated methods. Our approach is to find the "broken-symmetry" open-shell solution whenever possible and to use this geometry for higher-level calculations. In every case where an optimized geometry was located based on both a restricted (RDFT) and unrestricted solution (UDFT), the geometry based on the unrestricted solution produced a lower energy with single-point energies at the more rigorous level of theory.

On the bases of UDFT geometries, CASPT2 calculations[31] with the large atomic natural orbital (ANO-L) basis set[32] were carried out in order to include the effects of dynamic and nondynamic correlation.[33] The contraction schemes of the ANO-L basis set in this study were [4s3p2d] for nitrogen and [5s4p2d] for phosphorus. For diatomics such as N$_2$, P$_2$, and P≡N, an active space was chosen to include six electrons in six orbitals (6e,6o). For all tetraatomic P$_2$N$_2$ species, a 12-electron in 12-orbitals (12e,12o) active space was used. All CASPT2 calculations were made with the MOLCAS 5.0 program.[34] In Table 1, the CASPT2/ANO-L natural orbital occupation numbers of the HOMO and LUMO (the two orbital occupations which differ most from 2.0 and 0.0) are compared with ⟨S^2⟩ values at the UB3LYP/6-311+G(2df) level. In general, there is a good correlation between the HOMO or LUMO orbital population and ⟨S^2⟩. At the onset of symmetry breaking, where the UDFT solution is lower in energy than the restricted DFT (RDFT) solution, the CASPT2 HOMO occupation number is

about 1.8 electrons and the LUMO number is about 0.2 electrons. As the ⟨S^2⟩ value increases to that of a biradical (⟨S^2⟩ = 1.0), the CASPT2 HOMO and LUMO occupation numbers approach 1.0 (Table 1).

Results and Discussion

All possible structures in the tetraatomic P$_2$N$_2$ system were optimized (and frequencies calculated) at the standard DFT level. The labeling of minima (0 imaginary frequencies) and transition states (1 imaginary frequency) are as follows; bold letters refer to minima (i.e., "**A**" or "**B**"), "**TS**" designations with a number refer to transition states (i.e., "**TS1**" or "**TS2**"), while an asterisk indicates an open-shell singlet geometry (i.e., "**E***" or "**TS2***"). Computed relative energies at the DFT and CASPT2 levels are given in Table 1. Unless otherwise noted, relative energies will be at the CASPT2(12e,12o)/ANO-L//B3LYP/6-311+G(2df)+ZPC level, denoted as "CASPT2+ZPC". Optimized geometries of all minima on the tetraatomic P$_2$N$_2$ potential energy surface are shown in Figure 1 with calculated vibrational frequencies of stable minima given in Table 2. Total energies and Cartesian coordinates are available as Supporting Information.

Minimum **A**, a closed-shell butterfly structure with C_{2v} symmetry, is the lowest energy tetraatomic P$_2$N$_2$ species on the DFT potential energy surface (Figure 2). The P−N bond distance is computed to be 1.676 Å, compared to the known average P−N bond distance of 1.77 Å,[1] which is between the
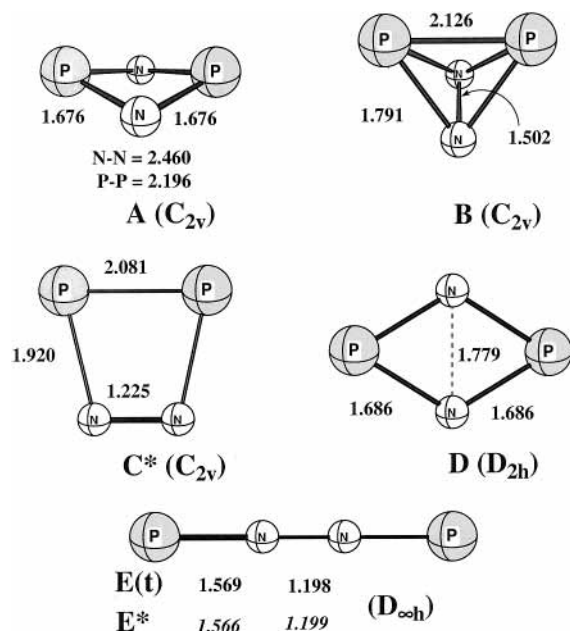
Figure 1. Optimized structures at the B3LYP/6-311+G(2df) level on the tetraatomic P_2N_2 PES.

computed N–N bond distance of N_4 (1.447 Å) and computed P–P bond distance of P_4 (2.200 Å).[17] The Wiberg bond indices (WBI)[35] in natural bond orbital (NBO)[36] analysis, a computational measure of bond order, indicates that the P–N bond is a typical single bond (WBI = 1.115). The N–N and P–P bond distances in **A** are computed to be 2.460 and 2.196 Å,

TABLE 2: Calculated Vibrational Frequencies (cm^{-1}) with Infrared Intensities in Parentheses (km/mol) for P_2N_2 Isomers at the B3LYP/6-311+G(2df) Level

	ν_1	ν_2	ν_3	ν_4	ν_5	ν_6
A (C_{2v})	369(11)	372(0)	644(8)	824(175)	877(17)	931(1)
B (C_{2v})	485(5)	585(3)	597(0)	627(0)	776(17)	980(11)
C* (C_{2v})	254(0)	341(0)	368(1)	560(0)	698(1)	1543(55)
D (D_{2h})	37(41)	493(32)	596(0)	848(0)	873(48)	887(0)
E* $(D_{\infty h})$	159(4)	383(0)	558(0)	1022(55)	1869(0)	
E(t) $(D_{\infty h})$	159(4)	380(0)	554(0)	1012(37)	1877(0)	

respectively. Minimum **B**, 2.0 kcal/mol higher in energy than **A** at the CASPT2+ZPC level, is the second lowest energy isomer with a closed-shell quasi-tetrahedral C_{2v} structure. The computed P–P bond (2.126 Å; WBI = 1.039), N–N bond (1.502 Å; WBI = 1.051), and P–N bond (1.791 Å; WBI = 0.889) show single-bond characters, while the P–P and N–N bonds are very similar to those in P_4 and N_4, respectively.[17] Minimum **C*** is 23.5 kcal/mol higher than **A**, with a small amount of biradical character (See Table 1, CASPT2 orbital occupation; 1.816 for HOMO, and 0.169 for LUMO). The P–P bond distance is computed to be 2.081 Å, indicating a single bond, whereas the N–N bond (1.225 Å) is slightly shorter than a typical N=N bond (1.25 Å[37]). In addition, the P–N bond distance (1.920 Å) in **C*** is rather long (P–N bond in **A** is 1.676 Å), which suggests that fragmentation may be facile. Minimum **D** is a closed-shell planar D_{2h} structure 31.7 kcal/mol higher in energy than **A** at the CASPT2 level. The computed P–N bond distance (1.686 Å) is very similar to that of minima **A** (1.676 Å), whereas the N–N bond is significantly longer than the N–N single bond in N_2H_4 (1.779 versus 1.45 Å).[1] Minimum **E(t)** is
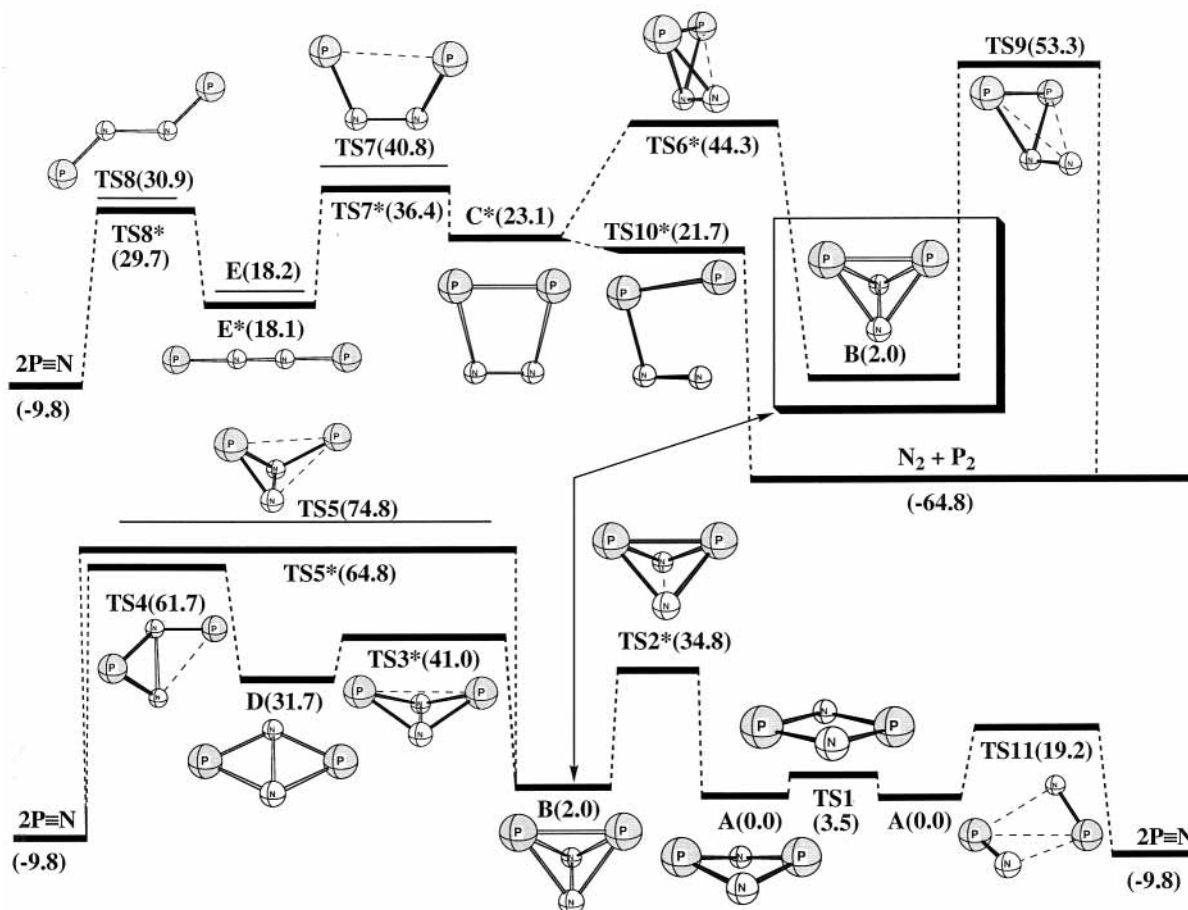

Figure 2. Potential energy surface (PES) of P_2N_2 system at the CASPT2+ZPC level (energies in kcal/mol relative to **A**). Structure **B** appears twice. A thin horizontal line indicates the CASPT2+ZPC value for the closed-shell (RDFT) geometry.
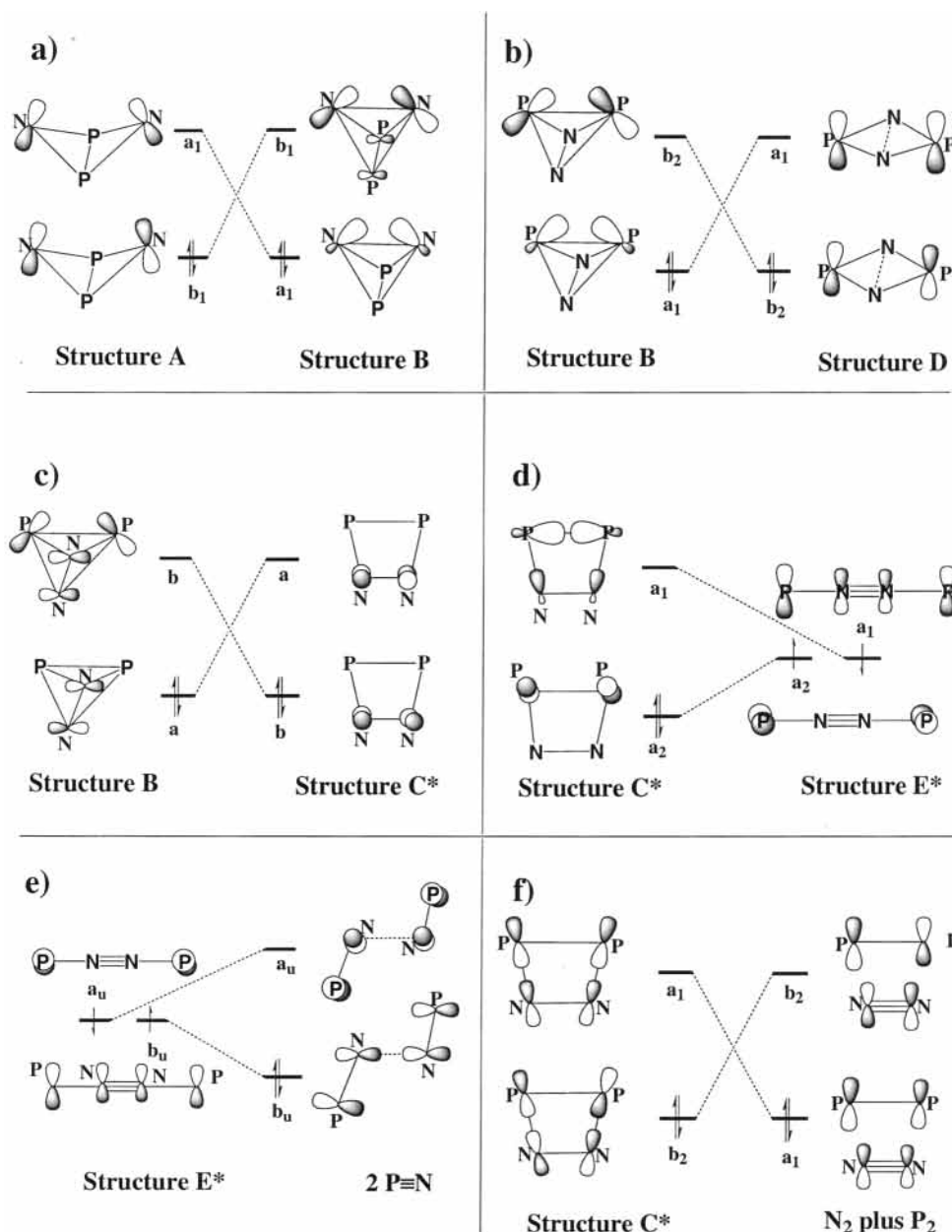
Structures and Reactions of P₂N₂

J. Phys. Chem. A, Vol. 106, No. 29, 2002 **6867**

Figure 3. Schematic depiction of orbital crossings between species on the P_2N_2 potential energy surface. (a) Molecular orbital correlation diagram between **A** and **B**, (b) between **B** and **D**, (c) between **B** and **C***, (d) between **C*** and **E***, (e) between **E*** and fragments (2P≡N), and (f) between **C*** and fragments (N_2 and P_2).

TABLE 3: Transition States Located for Reactions that Have an Orbital Crossing (see Figure 3)
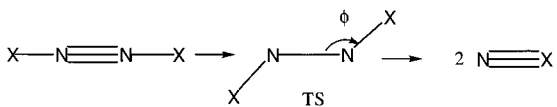
	figure	least motion symmetry	TS symmetry	$\langle S^2 \rangle$
TS2*	3a	C_{2v}	C_{2v}	0.85
TS3*	3b	C_{2v}	C_{2v}	0.98
TS6*	3c	C_2	C_1	1.00
TS7*	3d	C_{2v}	C_2	0.87
TS8*	3e	C_{2h}	C_{2h}	0.38
TS10*	3f	C_{2v}	C_s	0.34

a triplet which is only 4.9 kcal/mol higher in energy than **A** at the CASPT2+ZPC level, while the open-shell singlet (**E***) is 13.2 kcal/mol less stable than **E(t)**.

A number of reactions studied on the P_2N_2 PES have orbital crossings along the least-motion reaction paths. For six of the reactions (Figure 3), the orbitals that cross have been identified. In Table 3, the transition states for the six reactions in Figure 3 are listed along with the symmetry of the least-motion reaction path, the actual symmetry of the transition state, and the spin-

squared value. Three of the transition states (**TS6***, **TS7***, and **TS10***) have lower symmetries than the least-motion reaction path indicating the existence of stabilizing interactions allowed by mixing orbitals in the lower point group. In the reaction **C*** → **E*** (Figure 3d), the least motion path is C_{2v} during which the HOMO/LUMO switch from $a_1°a_2^2$ to $a_1^1a_2^1$. There is a C_{2v} → C_2 symmetry lowering in the transition state (**TS7***) which allows the a_1 and a_2 orbitals to mix (both have a symmetry in C_2 symmetry).

The reactions **C*** → **E*** and **E*** → 2P≡N (Figure 3d,e) do not actually involve an orbital crossing since the HOMO and LUMO on one side of the reaction become degenerate on the other side. The orbital crossing in the synchronous fragmentation of trapezoid **C*** to N_2 + P_2 (Figure 3f) is easily avoided by simply becoming unsymmetrical (**TS10***). In fact, the transition state **TS10*** is predicted to be 1.4 kcal/mol lower in energy than **C*** (Figure 2) which suggests that **C*** does not exist on

TABLE 4: Comparison of P−N≡N−P with ML₃−N≡N−ML₃ Complexes, M = Mo, W, and L = NH₂

X	X(Q−D)[a]	XNNX(T−S)[b]	N−N[c]	N−N(TS)[d]	NNX(TS)[e]	ΔH_a[f]	ΔH_{rxn}[g]	BDE(X/NNX)[h]
P	32.5	13.2	1.199	1.612	129.0	32.5	14.7	29.2
Mo(NH₂)₃[i]	14.5	6.4	1.220	1.544	140.0	14.5	26.9	48.5
W(NH₂)₃[i]	4.9	1.2	1.238	1.458	145.8	4.9	48.0	36.3

[a] Quartet−doublet splitting of X in kcal/mol. Quartet is ground state. [b] Triplet−singlet splitting of XNNX in kcal/mol. Triplet is ground state. [c] N−N distance (Å) in XNNX singlet minimum. [d] N−N distance (Å) in XNNX singlet transition structure. [e] N−N−X angle in XNNX singlet transition structure. [f] Activation barrier for singlet XNNX → 2 NX reaction in kcal/mol. [g] Exothermicity of dissociation reaction in kcal/mol. [h] Bond dissociation energy (kcal/mol) for the X−NNX bond with respect to triplet XNNX going to quartet plus doublet products. [i] Reference 40.
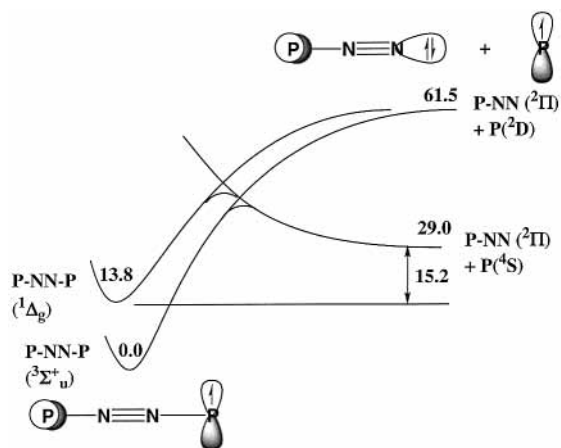
Figure 4. Potential energy curve showing an avoided crossing in the fragmentation of P−N≡N−P. The diabatic curve connects with PNN (²Π) plus P(²D) while the adiabatic curve connects PNN (²Π) plus P(⁴S). The energy of P(²D) was determined by adding the experiment quartet-doublet splitting (32.5 kcal/mol) to the CASPT2 calculated energy of P(⁴S). The crossing seam between the states was not located.

the potential energy surface. Thus, reactions which involve **C*** are predicted to go directly to N₂ + P₂.

The reaction of singlet P−N≡N−P (**E***) → 2P≡N is perhaps the most intriguing process because a formally triplet N≡N bond is broken in a single step with an activation barrier of only 11.6 kcal/mol. This reaction is of intense interest to nitrogen fixation where molecular nitrogen is converted by biological processes into ammonia.[38] The complex, (μ−N₂){Mo[N(R)Ar]₃}₂, R= CMe₃, and Ar = 3,5-C₆H₃Me₂, has been found to undergo nitrogen−nitrogen bond cleavage with an activation barrier of 23.3 ± 0.3 kcal/mol.[39] Morokuma and co-workers[40] undertook a theoretical investigation of this reaction with the model complexes, ML₃−N≡N−ML₃, M = Mo and W, and L = H, Cl, and NH₂. The present results are compared in Table 4 where replacing P with M(NH₂)₃, M = Mo and W, bares an uncanny similarity. The ground state of P and M(NH₂)₃ are quartets, the ground states of X−N≡N−X, X = P, M(NH₂)₃ are triplets, and the transition state for nitrogen fragmentation involves trans bending of the terminal groups. Trans bending allows a N−N π orbital to correlation with one component of the P≡N bond (Figure 3e).

If fragmentation of X−N≡N−X occurs stepwise, the lowest energy fragments, X and NNX, are in the quartet and doublet electronic states. However, the reaction correlates with the excited (²P) state of phosphorus (Figure 4) that is 32.5 kcal/mol higher than the ⁴S ground state.[41] At some point along the single-bond P−N fragmentation pathway, the ⁴S/²Π surface will intersect the ²P/²Π surface and be followed by intersystem crossing to the ground state. Since the ground-state fragments
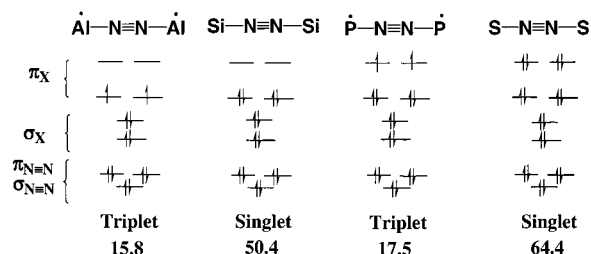
Figure 5. Molecular orbital diagram of X−N≡N−X, X = Al, Si, P, and S. The ground state for the linear species is a triplet for X = Al and P and a singlet for X = Si and S. The values below each MO set is the difference between the triplet and closed-shell singlet at the B3LYP/6-311+G(2dp)+ZPC level.

are calculated be to 15.2 kcal/mol higher than reactants with an undetermined addition activation along the adiabatic reaction surface, stepwise fragmentation is not expected to be competitive with concerted fragmentation which has an activation barrier of 11.6 kcal/mol.

The calculated N≡N bond distance in **E(t)** (1.198 Å) is only 0.1 Å longer than the N₂ triple bond (1.0975 Å).[42] The corresponding calculated N−N distances in M(NH₂)₃N≡NM-(NH₂)₃, M = Mo, and W, are slightly longer at 1.238 and 1.220 Å, respectively. The calculated N≡N stretching frequency in **E(t)** (ν(N≡N)=1869 cm⁻¹, Table 2) is also higher than the experimental ν(N≡N) in (μ−N₂){Mo[N(R)Ar]₃}₂ (1630 cm⁻¹).[39]

Prior calculations of linear AlNNAl (**X**),[43,44] SiNNSi (**Y**),[45] and SNNS (**Z**)[46] suggest an alternating pattern of ground state triplets and singlets for the linear species. To compare the XNNX, X = Al, Si, P, and S, series at a consistent level of theory, calculations have been made at the B3LYP/6-311+G-(2dp)+ZPC (Table 1). If comparison is made between the XNNX triplet and closed-shell singlet, the triplet is lower by 15.8 and 17.5 kcal/mol for X = Al and P, while the singlet is lower by 50.4 and 64.4 kcal/mol for X = Si and S. The explanation can easily be seen in a simple MO diagram (Figure 5). The N≡N triple bond is exceptional strong especially in comparison to bonding between N and Al, Si, P, or S. Thus, the biradical nature of Al−N≡N−Al (**X(t)**) and P−N≡N−P (**E(t)**) reflects the half-filled π level in the linear species (Figure 5).

The triplet state of P−N≡N−P (**E(t)**) is 13.2 kcal/mol lower in energy than the biradical singlet (**E***). In the case of Si−C≡C−Si, a system isoelectronic with Al−N≡N−Al, Rintelman and Gordon[47] found the linear triplet to be 4.6 kcal/mol more stable than the biradical singlet at the MCQDPT(12e,11o)/aug-cc-pVDZ+ZPE level. In P−N≡N−P or Si−C≡C−Si, the −X≡X− linkage allows conjugation between the two terminal atoms (phosphorus or silicon) such that the orbital of each unpaired electron has a tail residing on the opposite terminal

atom. Electron repulsion between one unpaired electron and the tail of the other is minimized if the spins are parallel, thus favoring the triplet state.

Conclusions

A comprehensive study of the P₂N₂ potential energy surface has been reported. The quasi-tetrahedral isomer **B** is predicted to be the most kinetically stable P₂N₂ species with a 32.8 kcal/mol activation barrier for fragmentation to two P≡N molecules. The most thermodynamically stable P₂N₂ isomer is a butterfly isomer **A**, which has a 19.2 kcal/mol barrier to form two P≡N molecules. A linear triplet P−N≡N−P isomer (**E(t)**) is only 4.9 kcal/mol higher than the tetraatomic global minimum (**A**). The most likely unimolecular barrier for decomposition of **E(t)** is intersystem crossing to the linear singlet (**E***), 13.2 kcal/mol higher in energy, followed by 11.6 kcal/mol of additional thermal activation for fragmentation via a trans-bent transition state to yield two P≡N molecules. An interesting alternating sequence of triplet and singlet ground states was found in the linear series XNNX, X = Al, Si, P, and S. The explanation is traced to the dominating stability of the N≡N triple bond and the sequence of half-filled/full-filled π orbitals as X varies from Al to S.

Supporting Information Available: B3LYP/6-311+G(2df) energies (hartrees), spin-squared values, zero-point energies (kcal/mol), heat capacity corrections to 298K (kcal/mol), entropies (cal/mol K), CAS(12e,12o)/ANO-L energies (hartrees), CASPT2/ANO-L energies (hartrees), and contribution to MP2 electron correlation from the active space for P₂N₂ species are given in Table S1 (1 page). Cartesian coordinates for P₂N₂ species optimized at the B3LYP/6-311+G(2df) level of theory are given in Table S2. This material is available free of charge via the Internet at http://pubs.acs.org.

References and Notes

(1) Greenwood, N. N.; Earnshaw, A. *Chemistry of the Elements*; Butterworth Heinemann: Boston, 1997.

(2) Francl, M. M.; Chesick, J. P. *J. Phys. Chem.* **1990**, *94*, 526.

(3) Lee, T. J.; Rice, J. E. *J. Chem. Phys.* **1991**, *94*, 1215.

(4) Lauderdale, W. J.; Stanton, J. F.; Bartlett, R. J. *J. Phys. Chem.* **1992**, *96*, 1173.

(5) Yarkony, D. R. *J. Am. Chem. Soc.* **1992**, *114*, 5406.

(6) Glukhovtsev, M. N.; Schleyer, P. v. R. *Int. J. Quantum Chem.* **1992**, *198*, 547.

(7) Dunn, K. M.; Morokuma, K. *J. Chem. Phys.* **1995**, *102*, 4904.

(8) Korkin, A. A.; Balkova, A.; Bartlett, R. J.; Boyd, R. J.; Schleyer, P. v. R. *J. Phys. Chem.* **1996**, *100*, 5702.

(9) Glukhovtsev, M. N.; Jiao, H.; Schleyer, P. v. R. *Inorg. Chem.* **1996**, *35*, 7124.

(10) Glukhovtsev, M. N.; Laiter, S. *J. Phys. Chem.* **1996**, *100*, 1569.

(11) Larson, Å; Larsson, M.; Östmark, H. *J. Chem. Soc., Faraday Trans.* **1997**, *93*, 2963.

(12) Leininger, M. L.; Van Huis, T. J.; Schaefer, H. F., III *J. Phys. Chem. A* **1997**, *101*, 4460.

(13) Bickelhaupt, F. M.; Hoffmann, R.; Levine, R. D. *J. Phys. Chem. A* **1997**, *101*, 8255.

(14) Perera, S. A.; Bartlett, R. J. *Chem. Phys. Lett.* **1999**, *314*, 381.

(15) Bittererová, M.; Brinck, T.; Östmark, H. *J. Phys. Chem. A* **2000**, *104*, 11999.

(16) Zheng, J. P.; Waluk, J.; Spanget-Larsen, J.; Blake, D. M.; Radziszewski, J. G. *Chem. Phys. Lett.* **2000**, *328*, 227.

(17) Hirsch, A.; Chen, Z.; Jiao, H. *Angew. Chem., Int. Ed.* **2001**, *40*, 2834.

(18) Östmark, H.; Launila, O.; Wallin, S.; Tryman, R. *J. Raman Spectrosc.* **2001**, *32*, 195.

(19) Bittererová, M.; Östmark, H.; Brinck, T. *Chem. Phys. Lett.* **2001**, *347*, 220.

(20) Woodward, R. B.; Hoffmann, R. *The Conservation of Orbital Symmetry*; Verlag Chemie Academic Press: Weinheim, 1970.

(21) Cacace, F.; de Petris, G.; Troiani, A. *Science* **2002**, *295*, 480.

(22) (a) Jones, R. O.; Hohl, D. *J. Chem. Phys.* **1990**, *92*, 6710. (b) Warren, D. S.; Gimarc, B. M. *J. Am. Chem. Soc.* **1992**, *114*, 5378. (c) Janoschek, R. *Chem. Ber.* **1992**, *125*, 2687. (d) Häser, M.; Schneider, U.; Ahlrichs, R. *J. Am. Chem. Soc.* **1992**, *114*, 9551. (e) Ballone, P.; Jones, R. O. *J. Chem. Phys.* **1994**, *100*, 4941. (f) Huang, R.; Li, H.; Lin, Z.; Yang, S. *J. Phys. Chem.* **1995**, *99*, 1418. (g) Häser, M.; Treutler, O. *J. Chem. Phys.* **1995**, *102*, 3703. (h) Scherer, O. J. *Angew. Chem., Int. Ed.* **2000**, *39*, 1029.

(23) (a) Ziurys, L. M. *Astrophys. J.* **1987**, *321*, L81. (b) Turner, B. E.; Bally, J. *Astrophys. J.* **1987**, *321*, L75. (c) Turner, B. E.; Tsuji, T.; Bally, J.; Guelin, M.; Cernicharo, J. *Astrophys. J.* **1990**, *365*, 569. (d) Adams, N. G.; McIntosh, B. J.; Smith, D. *Astron. Astrophys.* **1990**, *232*, 443.

(24) Atkins, R. M.; Timms, T. L. *Spectrochim. Acta* **1968**, *72*, 1611.

(25) (a) Ahlrichs, R.; Bär, M.; Plitt, H. S.; Schnöckel, H. *Chem. Phys. Lett.* **1989**, *161*, 179. (b) Schnöckel, H.; Mehner, T.; Plitt, H. S.; Schunck, S. *J. Am. Chem. Soc.* **1989**, *111*, 4578.

(26) (a) Parr, R. G.; Yang, W. *Density-Functional Theory of Atoms and Molecules*; Oxford University Press: Oxford, 1989. (b) Koch, W.; Holthausen, M. C. *A Chemist's Guide to Density Functional Theory*; Wiley-VCH: Weinheim, 2000.

(27) Becke, A. D. *J. Chem. Phys.* **1993**, *98*, 5648.

(28) MOLDEN: Schaftenaar G.; Noordik, J. H. *J. Comput.-Aided Mol. Des.* **2000**, *14*, 123.

(29) Frisch, M. J.; Trucks, G. W.; Schlegel, H. B.; Scuseria, G. E.; Robb, M. A.; Cheeseman, J. R.; Zakrzewski, V. G.; Montgomery, J. A., Jr.; Stratmann, R. E.; Burant, J. C.; Dapprich, S.; Millam, J. M.; Daniels, A. D.; Kudin, K. N.; Strain, M. C.; Farkas, O.; Tomasi, J.; Barone, V.; Cossi, M.; Cammi, R.; Mennucci, B.; Pomelli, C.; Adamo, C.; Clifford, S.; Ochterski, J.; Petersson, G. A.; Ayala, P. Y.; Cui, Q.; Morokuma, K.; Malick, D. K.; Rabuck, A. D.; Raghavachari, K.; Foresman, J. B.; Cioslowski, J.; Ortiz, J. V.; Stefanov, B. B.; Liu, G.; Liashenko, A.; Piskorz, P.; Komaromi, I.; Gomperts, R.; Martin, R. L.; Fox, D. J.; Keith, T.; Al-Laham, M. A.; Peng, C. Y.; Nanayakkara, A.; Gonzalez, C.; Challacombe, M.; Gill, P. M. W.; Johnson, B.; Chen, W.; Wong, M. W.; Andres, J. L.; Head-Gordon, M.; Replogle, E. S.; Pople, J. A. *Gaussian 98,* revision A.7; Gaussian, Inc.: Pittsburgh, PA, 1998.

(30) (a) Wang, S. G.; Schwarz, W. H. E. *J. Chem. Phys.* **1996**, *105*, 4641. (b) Goldstein, E.; Beno, B.; Houk, K. N. *J. Am. Chem. Soc.* **1996**, *118*, 6036. (c) Bettinger, H. F.; Schleyer, P. v. R.; Schreiner, P. R.; Schaefer, H. F., III In *Modern Electronic Structure Theory and Applications to Organic Chemistry*; Davidson, E. L., Ed.; World Scientific: London, 1997; pp 89−171. (d) Cramer, C. J. *J. Am. Chem. Soc.* **1998**, *120*, 6261. (e) Gräfenstein, J.; Kraka, E.; Cremer, D. *Chem. Phys. Lett.* **1998**, *288*, 593. (f) Goddard, J. D.; Chen, X.; Orlova, G. *J. Phys. Chem. A* **1999**, *103*, 4078. (g) Gräfenstein, J.; Hjerpe, A. M.; Kraka, E.; Cremer, D. *J. Phys. Chem. A* **2000**, *104*, 1748. (h) Orlova, G.; Goddard, J. D. *J. Phys. Chem.* **2000**, *112*, 10085. (i) Sevin, F.; McKee, M. L. *J. Am. Chem. Soc.* **2001**, *123*, 4591. (j) Prall, M.; Wittkopp, A.; Schreiner, P. R. *J. Phys. Chem. A* **2001**, *105*, 9265. (k) Prall, M.; Krüger, A.; Schreiner, P. R.; Hopf, H. *Chem. Eur. J.* **2001**, *7*, 4386. (l) Cremer, D. *Mol. Phys.* **2001**, *99*, 1899. (m) Bally, T.; Borden, W. T. In *Reviews in Computational Chemistry*; Lipkowitz, K. B., Boyd, D. B., Eds.; Wiely-Interscience: Chichester, 1988; p 1.

(31) Andersson, K.; Roos, B. O. *Int. J. Quantum Chem.* **1993**, *45*, 591.

(32) (a) Widmark, P.-O.; Malmqvist, P.-Å.; Roos, B. O. *Theor. Chim. Acta* **1990**, *77*, 291. (b) Widmark, P.-O.; Persson, B. J.; Roos, B. O. *Theor. Chim. Acta* **1991**, *79*, 419.

(33) Jensen, F. *Introduction to Computational Chemistry*; Wiley: New York, 1999.

(34) Andersson, K.; Barysz, M.; Bernhardsson, A.; Blomberg, M. R. A.; Carissan, Y.; Cooper, D. L.; Cossi, M.; Fleig, T.; Fülscher, M. P.; Gagliardi, L.; de Graff, C.; Hess, B. A.; Karlström, G.; Lindh, R.; Malmqvist, P.-Å.; Neogrády, P.; Olsen, J.; Roos, B. O.; Schimmelpfenning, B.; Schütz, M.; Seijo, L.; Serrano-Andrés, L.; Siegbahn, P. E. M.; Stålring, J.; Thorsteinsson, T.; Veryazov, V.; Wierzbowska, M.; Widmark, P.-O. *MOLCAS*, version 5.0; Lund University: Lund, Sweden, 2001.

(35) Wiberg, K. B. *Tetrahedron* **1968**, *24*, 1083.

(36) (a) Reed, A. E.; Weinstock, R. B.; Weinhold, F. *J. Chem. Phys.* **1985**, *83*, 735. (b) Reed, A.; Curtiss, L. A.; Weinhold, F. *Chem. Rev.* **1988**,

88, 899. (c) Weinhold, F. A. In *Encyclopedia of Computational Chemistry*; Schleyer, P. v. R., Ed.; Wiley Publishers: New York, 1998; Vol. 3; pp 1792−1810.

(37) Huheey, J. E.; Keiter E. A.; Keiter, R. L. *Inorganic Chemistry*, 4th ed.; HarperCollins College Publishers: New York, 1993.

(38) (a) Rees, D. C.; Howard, J. B. *Curr. Opin. Chem. Biol.* **2000**, *4*, 559. (b) Fryzuk, M. D.; Johnson, S. A. *Coord. Chem. Rev.* **2000**, *200*, 379.

(39) Laplaza, C. E.; Johnson, M. J. A.; Peters, J. C.; Odom, A. L.; Kim, E.; Cummins, C. C.; George, G. N.; Pickering, I. J. *J. Am. Chem. Soc.* **1996**, *118*, 8623.

(40) Cui, Q.; Musaev, D. G.; Svensson, M.; Sieber, S.; Morokuma, K. *J. Am. Chem. Soc.* **1995**, *117*, 12366.

(41) P(^{4}S)/P(^{2}D) splitting: NIST Atomic Spectra Database, NIST Standard Reference Database no. 78; http://physics.nist.gov.

(42) Wilkinson, P. G.; Houk, N. B. *J. Chem. Phys.* **1956**, *24*, 528.

(43) Boo. B. H.; Liu, Z. *J. Phys. Chem. A* **1999**, *103*, 1250.

(44) Andrews, L.; Zhou, M.; Chertihin, G. V.; Bare, W. D.; Hannachi, Y. *J. Chem. Chem. A* **2000**, *104*, 1656.

(45) Ornellas, F. R.; Iwata, S. *J. Phys. Chem.* **1996**, *100*, 16155.

(46) Warren, D. S.; Zhao, M.; Gimarc, B. M. *J. Am. Chem. Soc.* **1995**, *117*, 10345.

(47) Rintelman, J. M.; Gordon, M. S. *J. Chem. Phys.* **2001**, *115*, 1795.